articles

molecular pharmaceutics

System Dynamics of Subcellular Transport

Vivien Y. Chen,[†] Sonya M. Khersonsky,[‡] Kerby Shedden,[§] Young Tae Chang,[‡] and Gus R. Rosania*,[†]

Department of Pharmaceutical Sciences, University of Michigan College of Pharmacy, Ann Arbor, Michigan 48109, Department of Chemistry, New York University, New York, New York 10003, and Department of Statistics, University of Michigan, Ann Arbor, Michigan 48109

Received August 20, 2004

Abstract: In pharmacokinetic experiments, interpretations often hinge on treating cells as a "black box": a single, lumped compartment or boundary. Here, a combinatorial library of fluorescent small molecules was used to visualize subcellular transport pathways in living cells, using a kinetic, high content imaging system to monitor spatiotemporal variations of intracellular probe distribution. Most probes accumulate in cytoplasmic vesicles and probe kinetics conform to a nested, two-compartment dynamical system. At steady state, probes preferentially partition from the extracellular medium to the cytosol, and from the cytosol to cytoplasmic vesicles, with hydrophobic molecules favoring sequestration. Altogether, these results point to a general organizing principle underlying the system dynamics of subcellular, small molecule transport. In addition to plasma membrane permeability, subcellular transport phenomena can determine the active concentration of small molecules in the cytosol and the efflux of small molecules from cells. Fundamentally, direct observation of intracellular probe distribution challenges the simple boundary model of classical pharmacokinetics, which considers cells as static permeability barriers.

Keywords: Supertargeted chemistry; fluorescent probes; chemical biology; combinatorial chemistry; drug resistance; systems biology; high content screening

Introduction

Drug transport studies are an essential component of many drug discovery efforts, preclinical and clinical phases of pharmaceutical development and regulatory submissions. They involve assaying drug absorption, distribution, and clearance in cell-based, animal, and human studies.[1,2] Currently, there is a push to use cell-based high-throughput assays to replace animal studies, for predicting oral drug absorption, for predicting blood−brain barrier penetration, or for assessing the effect of specific membrane transporters on drug pharmacokinetics. In cancer cells, cell-based transport studies are important for assaying multidrug resistance phenotypes.[3−6] Integral membrane transporters like P-gly-

* Author to whom correspondence should be addressed: University of Michigan College of Pharmacy, 428 Church Street, Ann Arbor, MI 48109. E-mail: grosania@umich.edu. Tel: 734-763-1032. Fax: 734-615-6162.

[†] University of Michigan College of Pharmacy.

[‡] New York University.

[§] Department of Statistics, University of Michigan.

(1) Pritchard, J. F.; Jurima-Romet, M.; Reimer, M. L.; Mortimer, E.; Rolfe, B.; Cayen, M. N. Making better drugs: Decision gates in non-clinical drug development. *Nat. Rev. Drug Discovery* **2003**, *2*, 542−553.

(2) Sun, D.; Yu, L. X.; Hussain, M. A.; Wall, D. A.; Smith, R. L.; Amidon, G. L. In vitro testing of drug absorption for drug 'developability' assessment: forming an interface between in vitro preclinical data and clinical outcome. *Curr. Opin. Drug Discovery Dev.* **2004**, *7*, 75−85.

(3) Simon, S. M.; Schindler, M. Cell biological mechanisms of multidrug resistance in tumors. *Proc. Natl. Acad. Sci. U.S.A.* **1994**, *91*, 3497−3504.

(4) Gottesman, M. M.; Fojo, T.; Bates, S. E. Multidrug resistance in cancer: role of ATP-dependent transporters. *Nat. Rev. Cancer* **2002**, *2*, 48−58.

10.1021/mp049916t CCC: $27.50
Published on Web 10/23/2004

coprotein are overexpressed in cancer cells, rendering cells multidrug resistant by facilitating unidirectional transport of drugs across membranes.[3,4]

Generally, transporter proteins are believed to be present mostly at the plasma membrane to facilitate drug efflux from cells.[7] However, studies looking at the distribution of transporter proteins in tumors indicate that a substantial fraction of transporters are associated with membranes of intracellular vesicles.[8] Indeed, endocytic recycling of the plasma membrane can lead to the internalization of cell surface transporter proteins into intracellular vesicles. Also, transporter proteins are synthesized in the endoplasmic reticulum, traffic through the Golgi, and are present in exocytic vesicles that eventually fuse with the plasma membrane.[9−12]

However, the design and interpretation of pharmacokinetic experiments, as well as cell-based drug uptake and transport assays, often hinge on models that treat cells as compartment boundaries, or as single, lumped compartments. Therefore, we began to consider strategies for characterizing the endogenous small molecule transport mechanisms at the subcellular level. This effort was also prompted by studies of paclitaxel pharmacokinetics, indicating an important role of intracellular drug binding in the response of tumors to this anticancer agent,[5,6,13] and by studies indicating that transporters present in intracellular vesicles are functional.[14,15]

Fluorescent transporter probes accumulate in cytoplasmic vesicles laden with transporter proteins, suggesting that sequestration of small molecules inside intracellular vesicles may influence cellular transport processes.[14] Nevertheless, studies performed to date have not quantitatively distinguished the partitioning of probes from the cytosol to intracellular vesicles or from cytosol to the extracellular medium. Since transfection of cells with transporter−GFP chimeras could also alter the endogenous transport mechanisms complicating interpretation of experiments, we decided to begin assessing the endogenous transport properties of intracellular vesicles and plasma membranes of live, untransfected cells, using fluorescent probes to directly monitor probe sequestration.

For this purpose, a kinetic, high content screening system[16] was used to image the spatiotemporal kinetics of fluorescent probe distribution in microscopic images of cells. Using a combinatorial library of fluorescent triazine derivatives, the partition coefficients between the extracellular medium and the cytosol and between the cytosol and cytoplasmic vesicles were calculated. Monitoring the transport of a chemically diverse collection of probes sharing similar fluorescent properties allows us to make statistically meaningful inferences about the relationship between chemical structure and subcellular transport. Accounting for global trends in the data, small molecules partition between the extracellular medium and the cytosol, followed by partitioning of the molecules from the cytosol into cytoplasmic vesicles. Across the entire library, probes that partition from the cytosol into vesicles preferentially partition from the cytosol to the extracellular medium. The observations demonstrate that, while pharmacokinetic experiments allow inferences to be made about intracellular transport processes, fluorescent small molecules can be used to directly track subcellular transport pathways in living cells.

Materials and Methods

Tagged NBD Library Synthesis. Procedure for Building Block I Synthesis (Figure S1b, Supporting Information). Eight amines (R_2 = A−H, Figure 1) (0.44 mmol, 5 equiv) were added to a suspension of PAL-aldehyde resin (80 mg, 0.088 mmol) in anhydrous tetrahydrofuran (THF) (5 mL containing 2% of acetic acid) at room temperature. The reaction mixture was shaken for 1 h at room temperature followed by addition of sodium triacetoxyborohydride (131 mg, 7 equiv). The reaction mixture was stirred for 12 h and filtered. The resin was washed with DMF (5 times), alternatively with dichloromethane and methanol (5 times), and finally dichloromethane (5 times). The resin was dried in a vacuum.

(5) Jang, S. H.; Wientjes, M. G.; Au, J. L. Determinants of paclitaxel uptake, accumulation and retention in solid tumors. *Invest. New Drugs* **2001**, *19*, 113−123.
(6) Jang, S. H.; Wientjes, M. G.; Au, J. L. Interdependent effect of P-glycoprotein-mediated drug efflux and intracellular drug binding on intracellular paclitaxel pharmacokinetics: application of computational modeling. *J. Pharmacol. Exp. Ther.* **2003**, *304*, 773−780.
(7) Schinkel, A. H.; Jonker, J. W. Mammalian drug efflux transporters of the ATP binding cassette (ABC) family: an overview. *Adv. Drug Delivery Rev.* **2003**, *55*, 3−29.
(8) Meschini, S.; Calcabrini, A.; Monti, E.; Del Bufalo, D.; Stringaro, A.; Dolfini, E.; Arancia, G. Intracellular P-glycoprotein expression is associated with the intrinsic multidrug resistance phenotype in human colon adenocarcinoma cells. *Int. J. Cancer* **2000**, *87*, 615−628.
(9) Molinari, A.; Calcabrini, A.; Meschini, S.; Stringaro, A.; Del Bufalo, D.; Cianfriglia, M.; Arancia, G. Detection of P-glycoprotein in the Golgi apparatus of drug-untreated human melanoma cells. *Int. J. Cancer* **1998**, *75*, 885−893.
(10) Abbaszadegan, M. R.; Cress, A. E.; Futscher, B. W.; Bellamy, W. T.; Dalton, W. S. Evidence for cytoplasmic P-glycoprotein location associated with increased multidrug resistance and resistance to chemosensitizers. *Cancer Res.* **1996**, *56*, 5435−5442.
(11) Conner, S. D.; Schmid, S. L. Regulated portals of entry into the cell. *Nature* **2003**, *422*, 37−44.
(12) Royle, S. J.; Murrell-Lagnado, R. D. Constitutive cycling: a general mechanism to regulate cell surface proteins. *Bioessays* **2003**, *25*, 39−46.
(13) Kuh, H. J.; Jang, S. H.; Wientjes, M. G.; Au, J. L. Computational model of intracellular pharmacokinetics of paclitaxel. *J. Pharmacol. Exp. Ther.* **2000**, *293*, 761−770.
(14) Rajagopal, A.; Simon, S. M. Subcellular localization and activity of multidrug resistance proteins. *Mol. Biol. Cell* **2003**, *14*, 3389−3399.
(15) Rajagopal, A.; Pant, A. C.; Simon, S. M.; Chen, Y. In vivo analysis of human multidrug resistance protein 1 (MRP1) activity using transient expression of fluorescently tagged MRP1. *Cancer Res* **2002**, *62*, 391−396.
(16) Abraham, V. C.; Taylor, D. L.; Haskins, J. R. High content screening applied to large-scale cell biology. *Trends Biotechnol.* **2004**, *22*, 15−22.

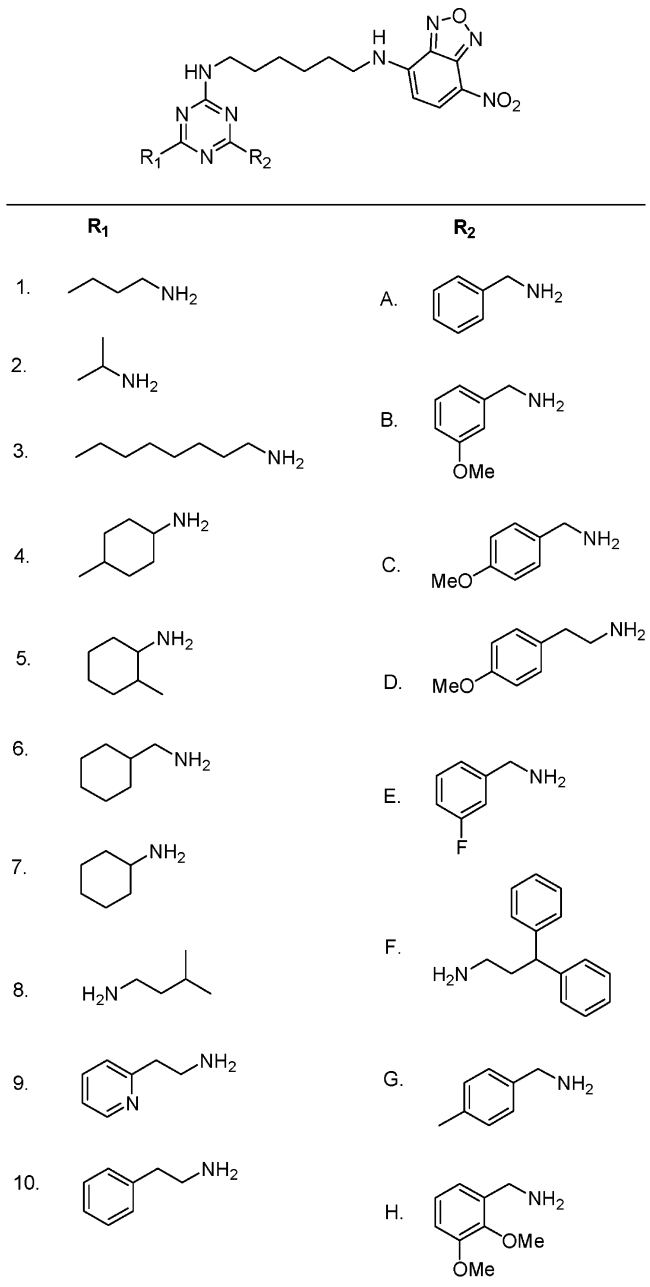

Figure 1. An NBD-tagged library of subcellular transport probes. Probes incorporate an NBD linker attached to a triazine scaffold derivatized at the R_1 position with groups 1−10 and R_2 position with groups A−H.

Procedure for Synthesis of NBD Linker (Figure S1a). To a solution of 1,6-hexanediamine (2.3 g, 20 mmol, 2 equiv) in methanol (150 mL) cooled to 0 °C and purged with nitrogen gas was added a solution of 4-chloro-7-nitrobenzofurazan (NBD chloride) (2 g, 10 mmol) in 100 mL of methanol dropwise over the period of 3 h. The solution was stirred for an additional hour, and then the solvent was removed in vacuo. The product, **1**, was purified by column chromatography (5:1 dichloromethane:methanol) to result in a yellow oil (1.9 g, 68% yield). The identity and purity of the final product was confirmed by LC−MS at 250 nm (Agilent 1100 model). ESIMS: $(M + H)^+$ calcd, 280.1; found, 280.1.

Procedure for Building Block II Synthesis. NBD linker, **1** (1.7 g, 1.2 equiv), was added to a solution of cyanuric chloride (1 g, 5 mmol) in THF (20 mL) and *N*,*N*-diisopropylethylamine (DIEA) (4.7 mL, 5 equiv) at 0 °C. The reaction mixture was stirred for 30 min at 0 °C. After the reaction progress was monitored by TLC, the reaction mixture was filtered through a silica plug and solvent was removed in vacuo. The reaction mixture was purified by column chromatography (1:1 ethyl acetate:hexanes) to result in a yellow oil (1.1 g, 48% yield). Its purity and identity were confirmed by LC−MS at 250 nm (>99% purity). ESIMS: $(M + H)^+$ calcd, 426.1; found, 426.1.

General Procedure for Coupling Building Block I and Building Block II. Building block II (0.26 mmol) was added to a solution of building block I (0.088 mmol) in DIEA (1 mL) and anhydrous THF (3 mL). The reaction mixture was heated to 60 °C for 3 h and filtered. The resin was washed with DMF (5 times), alternatively with dichloromethane and methanol (5 times), and finally dichloromethane (5 times). The resin was dried in a vacuum.

General Procedure for the Final Amination on the Resin and Product Cleavage Reaction. Ten amines (R_1 = 1−10, Figure 1) (4 equiv) were added to the resin (each 10 mg), coupled with building block I and building block II, in DIEA (8 μL) and 1 mL of *N*-methyl-2-pyrrolidone (NMP). The reaction mixture was heated to 120 °C for 3 h. The resins were washed with DMF (5 times), alternatively with dichloromethane and methanol (5 times), and finally dichloromethane (5 times). The resins were dried in a vacuum. The product cleavage reaction was performed using 5% TFA in dichloromethane (1 mL) for 30 min at room temperature and washed with dichloromethane (0.5 mL). The products were characterized by LC−MS at 250 nm (Agilent 1100 model).

Cell Culture. HeLa cells were grown in RPMI + 10% FCS in a 5% CO_2 atmosphere at 37 °C and plated in Falcon, tissue culture coated 96-well plates at a density of 3000 cells/well, 24 h prior to the start of the experiment.

Kinetic Imaging. For influx experiments, cells on 96-well plates were switched to imaging media consisting of RPMI containing 1.0 mM bromophenol blue filtered through a 0.2 μm membrane, 10 μM probe, and 0.1 μM Hoechst 33258 to label the cell nuclei. Bromophenol blue has a minimal effect on cell viability but allows visualizing extracellular probe (G.R., unpublished observation). Plates were then transferred to a KineticScan instrument (Cellomics, Inc., Pittsburgh, PA), which contains an environmentally controlled CO_2/temperature/humidity chamber, and data was acquired with a 20× objective lens. Image acquisition began approximately 10 min after dye addition, using the Hoechst filter set to acquire nuclear images and FITC filter set to acquire the NBD image. The plate-scanning mode was used for scanning, in which the instrument builds time-stacks of images by scanning the plate multiple times, returning to the same site of the plate at every scan. For efflux

experiments, dye-containing medium was removed from the wells of the plate. The wells were washed twice with fresh RPMI medium, imaging medium was added, and image acquisition was restarted 7 min after the dye-containing medium was removed. The last time points of the influx experiment served as the first time point of the efflux experiment. Plates were scanned for approximately 2 h in the influx experiment and 6 h for the efflux experiment, with each well imaged at approximately 7 min intervals, on average. Negative controls included unlabeled cells, which yielded no data on either channel, or Hoechst-only labeled cells, which yielded background noise data on the FITC channel. Short exposure times minimized photobleaching (1 s for FITC; 0.1 s for Hoechst). In addition, we confirmed that photobleaching exerted a minimal effect ($\ll$1%) on fluorescence intensity.

Image Analysis. Image data was analyzed using Metamorph image analysis software (Molecular Devices, Inc.). The entire image dataset was visually inspected for artifacts that would lead to changes in the measured fluorescence intensity independent of probe sequestration, such as cell rounding, autofocus errors, lack of image register, lack of cells in image, instrument malfunction, or some other experimental artifact. Approximately 20−40 cells were analyzed in each image. Because of acquisition error at the edge of the plate, data was not successfully acquired for probes C10, D10, E10, G10, H4, H7, H9, and H10. An image analysis algorithm[17] was programmed, so as to automatically analyze the intensity distribution of pixels in a perinuclear ring region of each cell in an image (Figure S2, Supporting Information). For this purpose, nuclear images were binarized and used to generate a perinuclear ring binary mask (Figure S2A), which was then utilized to determine the CV of the FITC channel (NBD) image (Figure S2B). The CV is the ratio of the standard deviation of the pixel intensities divided by the average pixel intensity and effectively represents the heterogeneity of intracellular probe distribution, as visually determined by a naive observer (data not shown). To create the perinuclear ring masks, the nuclear image obtained through the Hoechst channel was auto-thresholded for light objects (1, Figure S2A) and then binarized to create a nuclear mask (2, Figure S2A). The nuclear mask was dilated five pixels to create a NucDilate mask (3, Figure S2A). Independently, the nuclear mask was also inverted and skeletonized to create a watershed image (4, 5, Figure S2A). Next, the dilated and inverted/skeletonized images were combined using the Logical XOR function yielding a cell mask (6, Figure S2A). This cell mask was combined with the nuclear binary mask using the XOR function to create the perinuclear ring mask (7, Figure S2A). The ring mask image was then eroded one pixel to remove the skeletons (8, Figure S2A). Last, the cytoplasmic images obtained through the FITC channel were combined with the ring mask image using the Logical XAND function to create perinuclear ring mask images (Figure S2B). The perinuclear ring mask images were then auto-thresholded for light objects, and the average intensity and standard deviation of each image in its entirety were used to calculate the CV.

Mathematical Modeling A 4-parameter compartmental model was specified for the underlying vesicular and cytoplasmic probe concentrations. This model specified three compartments linked by first-order kinetics. The "medium" compartment is linked to the "cytoplasm" compartment via first-order rate constants $k(\text{cyto})_{\text{in}}$ and $k(\text{cyto})_{\text{out}}$, and the "cytoplasm" compartment is linked to the "vesicle" compartment via first-order rate constants $k(\text{ves})_{\text{in}}$ and $k(\text{ves})_{\text{out}}$. Probe concentration in the medium was fixed at 1 unit during influx and 0 units during efflux. For initial conditions, probe concentrations at time zero in both cytoplasm and vesicles were fixed at zero units, and concentration trajectories were constrained to be continuous over the boundary between influx and efflux conditions.

For specified values of the four kinetic parameters $k(\text{cyto})_{\text{in}}$, $k(\text{cyto})_{\text{out}}$, $k(\text{ves})_{\text{in}}$, and $k(\text{ves})_{\text{out}}$, and for the initial conditions stated above, probe concentrations of an ideal probe in cytoplasm and vesicles are uniquely determined as a sum of exponential curves, which can be numerically calculated using standard methods for solving systems of ordinary differential equations. We will write $V(t;K)$ and $C(t;K)$ to denote the solutions for vesicular and cytoplasmic concentrations at time t, where K is the four-dimensional vector of kinetic parameters.

Statistical Analysis of Kinetic Data. From the images, coefficients of variation (CV) of pixel intensities were analyzed in the context of the hypothetical, system dynamic model described above. Since we do not measure the compartmental concentrations directly, but rather observe the CV of pixel intensities, it is also necessary to model the link between the statistical distribution of pixel intensities and compartmental concentrations. To develop this link we considered a statistical model in which fraction p of the perinuclear image pixels were in vesicles and fraction $1 - p$ were not in vesicles. We supposed that vesicle pixels had intensity proportional to $V(t;K)$, and nonvesicle pixels had intensity proportional to $C(t;K)$, as defined above. Further, we supposed that the image was subject to independent Poisson noise at intensity λ. Under these assumptions, the standard deviation of the pixels is proportional to $((V(t;K) - C(t;K))^2 p(1 - p) + \lambda)^{1/2}$ and the mean of the pixels is proportional to $pV(t;K) + (1 - p)C(t;K) + \lambda$. Thus the ideal CV is

$$CV_{\text{mod}}(t;K,p,\lambda) = ((V(t;K) - C(t;K))^2 p(1 - p) + \lambda)^{1/2} / (pV(t;K) + (1 - p)C(t;K) + \lambda)$$

where the unknown constants of proportionality cancel in the ratio.

Experimental CV data were fitted to the six-parameter model (four kinetic parameters and the "system parameters"

(17) Ding, G. J.; Fischer, P. A.; Boltz, R. C.; Schmidt, J. A.; Colaianne, J. J.; Gough, A.; Rubin, R. A.; Miller, D. K. Characterization and quantitation of NF-kappaB nuclear translocation induced by interleukin-1 and tumor necrosis factor-alpha. Development and use of a high capacity fluorescence cytometric system. *J. Biol. Chem.* **1998**, *273*, 28897−28905.

p and λ) on the basis of the least squares principle. That is, the function $\sum_t(CV_{obs}(t) - CV_{mod}(t;K,p,\lambda))^2$ was minimized with respect to K, p, and λ for each probe. Optimization was carried out using simulated annealing.[18] Solutions in which cytoplasmic concentration exceeds vesicular concentration at steady state were discarded and a new solution was generated.

Estimation of Probe Permeability and Assessment of Estimation Precision. Because of the mathematical function linking actual probe concentrations with the fluorescence intensity apparent in the images, the optimization process generally yielded several different kinetic solutions of similarly good fit to the data. To summarize variation in kinetic parameter estimates across the good solutions, we ran the optimizer 100 times for each probe. Focusing on the best fits, we selected the solutions that were within 5% of the best fit. Within this selected set we plotted $\log[k(\text{cyto})_{in}/k(\text{cyto})_{out}]$ against $\log[k(\text{ves})_{in}/k(\text{ves})_{out}]$ for each probe and assessed the trend observed across all probes. Curve fits and observed relationship between P_{ap}(ves) and P_{ap}(cyto) were confirmed in an independent experiment.

Results

A novel library of 80 fluorescent-tagged triazine compounds was synthesized using our previously developed orthogonal chemistry pathway (Figure S1). In the design of this library, we combined the tagged-triazine library approach, where all library compounds contain a built-in linker,[19] with the internal-tagged, dye library approach.[20] Thus, an NBD moiety was attached to a six-carbon linker; then the resulting NBD linker was tethered to the triazine scaffold. The scaffold was then diversified at the R_1 and R_2 positions, resulting in 80 final compounds (Figure 1). The purity and identity of all the final products were monitored by LC−MS, and more than 90% of the compounds demonstrated >90% purity. This fluorescent-tagged library approach allows for facile high-throughput organelle directed screening.

For kinetic analysis, an automated, high content screening instrument equipped with an environmental chamber[16] was used to track intracellular probe sequestration, as cells were incubated with the fluorescent molecules and after removal of extracellular probe. A nontoxic, plasma membrane impermeant chromophore (bromophenol blue) was used to specifically suppress background signal. By masking background fluorescence, the extent of intracellular probe sequestration in cells became readily apparent even in the continuous presence of extracellular probe (Figure 2). Since the size of the fluorescent probes (MW <1000) is below the cutoff size of the nuclear pores (MW >10000), nuclear and cytosolic probe concentrations should equilibrate. Yet, most cells revealed marked fluorescence accumulation in the cytoplasm, and in many cells, the individual cytoplasmic vesicles where probe was sequestered were clearly visible (Figure 2A). Confocal microscopy of cells labeled with selected probes supports these observations (data not shown). Visually, many probes reach steady state levels of probe sequestration as soon as 10 min after beginning of incubation, with others showing more gradual sequestration (Figure 2B).

When probe was removed from the extracellular medium, a rapid efflux of probe was readily apparent (Figure 3). Because of the rapid efflux kinetics in the presence of a steep concentration gradient, intracellular probe sequestration was mostly apparent when extracellular probe was present in the medium (Figure 2). In the set of compounds we tested, only probes containing $R_1 = 3$ show significant retention in cytoplasmic vesicles, under efflux conditions (Figure 3). Since the $R_1 = 3$ group is the longest alkyl group represented in the library, this result would be consistent with membrane partitioning slowing down efflux kinetics. Fixed endpoint analysis confirms that probes possessing the $R_1 = 3$ group are avidly retained in intracellular vesicles regardless of which R_2 group was present (Figure 3B,C). Cells treated with probes containing $R_1 = 3$ exhibited CV values that were significantly higher than those of other R_1 groups 25 min after probe removal from the extracellular medium (Figure 3B; Table S1, Supporting Information) and independently of the starting amount of sequestered probe (Figure 3C).

On the basis of these observations, a hypothetical transport model was postulated, representing cells as a nested, two-compartment dynamical system (Figure 4). Parsimony led us to consider the simplest version of this model. Accordingly, the sequestration of probe in the cytosol and intracellular vesicles is described by a set of first-order differential equations, according to which probe concentration in the cytosol and vesicle compartment is related to the concentration of probe in the extracellular medium. The change in probe concentration in cytosol and vesicles is modeled as a function of the amount of time cells are in the presence or absence of extracellular probe, and to a four-dimensional kinetic vector describing the rate of probe influx and efflux between extracellular medium and cytosol, and the rate of probe influx and efflux between cytosol and intracellular vesicles.

Quantitative analysis of probe kinetics in relation to the hypothetical transport model indicates that overall probe behavior conforms to this nested, two-compartment dynamical system (Figure 5). For monitoring sequestration, image data was analyzed using image analysis software, measuring the statistical pixel intensity distribution associated with fluorescent probe sequestration in the perinuclear region[17] (Figure S2). Data were parametrized with a nested, two-compartment, transport model,[21] using a statistical link function to relate the CV of pixel intensities in the perinuclear

(18) Pincus, M. *Oper. Res.* **1979**, *18*, 1225.
(19) Khersonsky, S. M.; Jung, D. W.; Kang, T. W.; Walsh, D. P.; Moon, H. S.; Jo, H.; Jacobson, E. M.; Shetty, V.; Neubert, T. A.; Chang, Y. T. Facilitated forward chemical genetics using a tagged triazine library and zebrafish embryo screening. *J. Am. Chem. Soc.* **2003**, *125*, 11804−11805.
(20) Rosania, G. R.; Lee, J. W.; Ding, L.; Yoon, H. S.; Chang, Y. T. Combinatorial approach to organelle-targeted fluorescent library based on the styryl scaffold. *J. Am. Chem. Soc.* **2003**, *125*, 1130−1131.

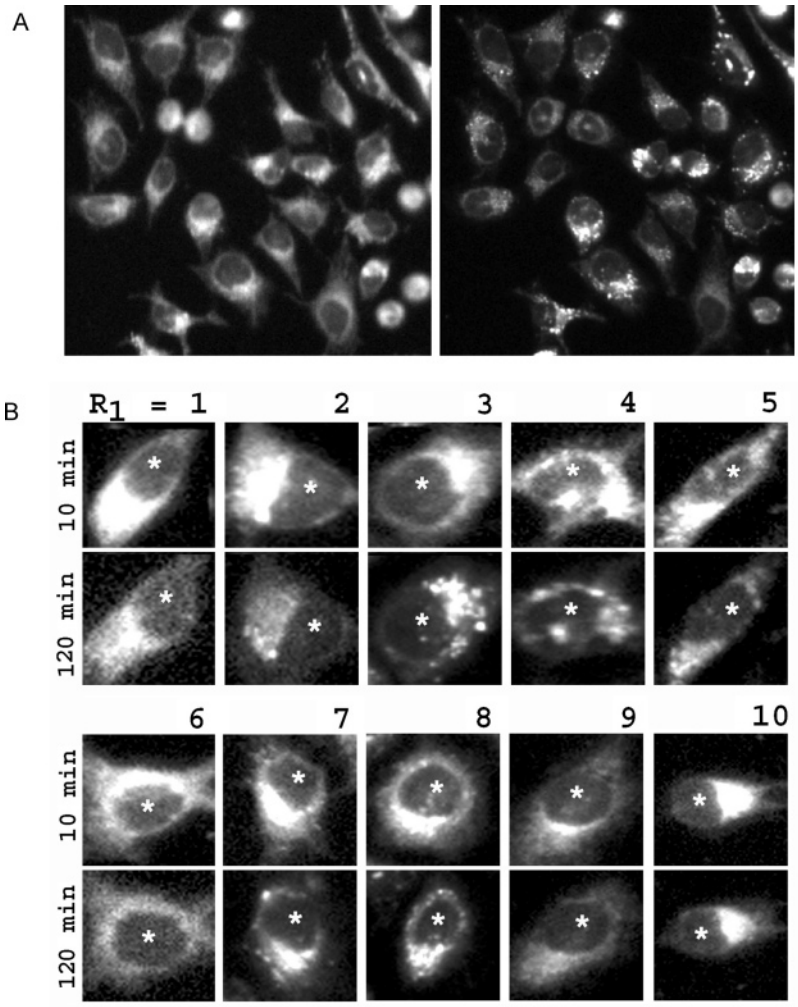

Figure 2. Images of cells showing cytoplasmic probe sequestration, acquired with a kinetic high content screening instrument. (A) Image of cells incubated with probe A3 at 10 min (left) and 1 h (right) after addition of probe. (B) Image of cells incubated with 10 different probes, incorporating the indicated group at the R_1 position, with the R_2 position held constant. Two images of each cell are shown, illustrating probe distribution 10 and 120 min after beginning of incubation.

region with the concentration of probe in vesicles and cytoplasm. Optimal kinetic parameters fitting the experimental data for each probe to the system described by the two-compartment model and statistical link function were determined using the simulated annealing technique.[18]

As can be observed from the kinetic traces acquired (Figure 5), there was a significant amount of variation in terms of the behavior of the probes, as recorded in the measured CV values of the image data. Many probes appeared to reach steady state distribution values before the first experimental time point was acquired, approximately 10 min after beginning of incubation of cells with probes. Others showed a more gradual increase in CV values, gradually reaching a plateau value as the experiment progressed. To quantitatively assess how well the model accounts for all the different kinetic traces acquired, the "PVE" (proportion of variance explained) by the model was calculated. The PVE is 1 minus the ratio of the sum of squared differences between observed and fitted values to the sum of squared differences between observed values and their mean. PVE values close to 1 indicate good fit to the nested, two-compartment model. The average PVE across the probes was 0.92, with >50% of the probes yielding PVE values ≥0.95, indicating an excellent fit to the data (Figure 5).

According to the parameter values used to calculate the optimal curve fits, it was possible to obtain a measure for the apparent partition coefficient between cytosol and intracellular vesicles ($P_{ap}(\text{ves}) = k(\text{ves})_{in}/k(\text{ves})_{out}$) and the apparent partition coefficient between extracellular medium and cytosol ($P_{ap}(\text{cyto}) = k(\text{cyto})_{in}/k(\text{cyto})_{out}$). Interestingly, these values were inversely related to each other, across compounds representing a variety of chemical structures (Figure 6). With the exception of three outliers (compounds D9, F9, and B9), log P_{ap}(ves) and log P_{ap}(cyto) values followed an approximately linear relationship (Figure 6). The outliers are

(21) Evans, W. E.; Schentag, J. J.; Jusko, W. J. *Applied Pharmacokinetics: Principles of Therapeutic Drug Monitoring*; Lippincott Williams & Wilkins: Vancouver, WA, 1992.

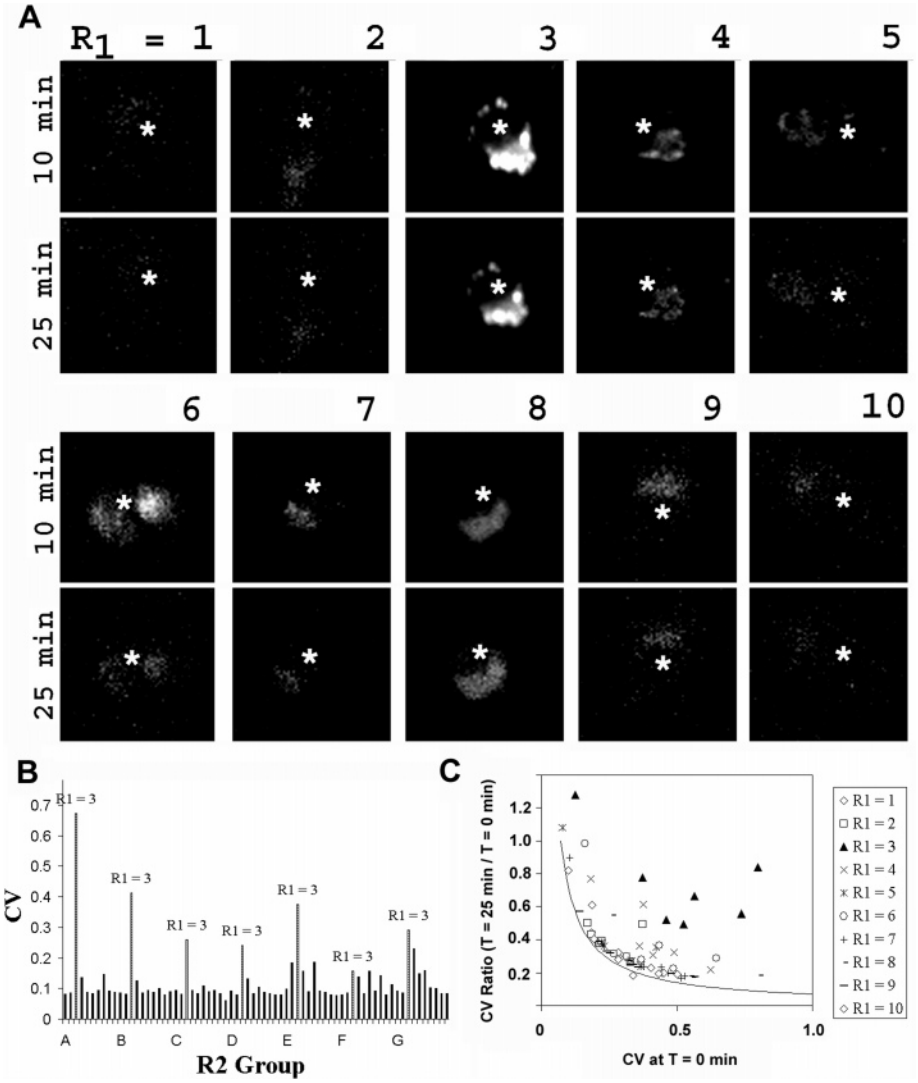

Figure 3. Images of cells acquired after removal of extracellular probe. (A) Under efflux conditions, probes derivatized with $R_1 = 3$ exhibit the greatest retention in intracellular compartments, as monitored 10 and 25 min after removal of probe from extracellular medium. Most other sequestered probes exhibit little retention, as soon as 10 min after removal of probe from extracellular medium. (B) The CVs of cells treated with $R_1 = 3$ derivatized probes 25 min after probe removal were consistently higher than the CVs of cells treated with probes derivatized with the other R_1 groups regardless of the R_2 group present. (C) Independent of the initial degree of probe sequestration, $R_1 = 3$ probes display greater retention than other probes in the library. The solid curve represents the values that would be expected if the probe had completely leaked from the cell, for different degrees of sequestration immediately prior to removal of extracellular probe.

all pyridine derivatives ($pK_a \approx 6.0$), so their P_{ap}(ves) and P_{ap}(cyto) values possibly reflect increased sequestration due to accumulation of pyridinium ions in acidic vesicles. Including all the compounds in the calculation of the correlation coefficient, the correlation is -0.56, which is highly significant. Excluding the three outliers, the correlation is -0.91.

This global trend indicates that differences in probe permeability of the intracellular compartment boundary where the probe is sequestered parallel differences in plasma membrane permeability. Consequently, small molecules that favor partitioning into the extracellular medium tend to be the ones that are most avidly sequestered intracellularly, and vice versa. Topologically, the lumen of the intracellular vesicles corresponds to the outside of the cell, which would explain why the correlation between log P_{ap}(ves) and log P_{ap}(cyto) is negative, if both share similar transport mechanisms.

These results also suggest that probe sequestration plays an important role in modulating cytosolic probe concentrations. The log P_{ap}(cyto) is positive for most probes (Figure 6), meaning that most probes tend to accumulate in the cytosol relative to the extracellular medium. Yet, because the log P_{ap}(ves) is also positive for most of the probes, molecules in the cytosol tend to become sequestered in intracellular vesicles. This explains why the amount of probe fluorescence in the nucleus is less than probe fluorescence in the cytoplasm (Figure 2). For this particular set of probes,

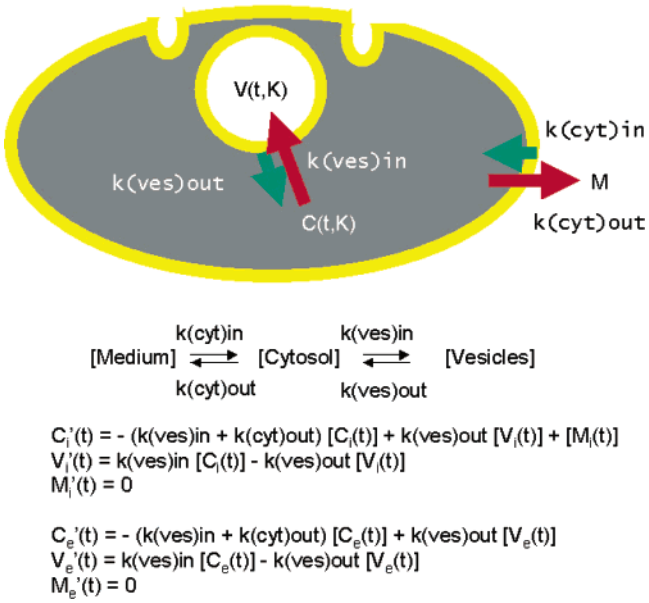

Figure 4. System dynamics of subcellular transport. A nested, two-compartment model was used to parametrize the subcellular transport properties of the probes in terms of four kinetic parameters: $k(\text{cyto})_{in}$, the rate at which probe enters the cytosol; $k(\text{cyto})_{out}$, the rate at which probe leaves the cytosol; $k(\text{ves})_{in}$, the rate at which the probe enters the vesicles; and $k(\text{ves})_{out}$, the rate at which the probe leaves the vesicles. In the illustration, a yellow line represents the plasma membrane, and gray represents the cytosol. The time evolution of the system is described by influx functions $C_i'(t)$ (cytoplasm), $V_i'(t)$ (vesicles), and $M_i'(t)$ (medium) and efflux functions $C_e'(t)$ (cytoplasm), $V_e'(t)$ (vesicles), and $M_e'(t)$ (medium).

there was little net efflux of probes up a concentration gradient from the cytosol to the extracellular medium. Yet probes do accumulate up a concentration gradient inside cytoplasmic vesicles. In images of individual cells, probe concentration in cytoplasmic vesicles appears to be greater than probe concentration in the rest of the nucleus or the cytoplasm, suggesting that the partitioning of probe in intracellular vesicles serves as a buffer for cytosolic probe concentrations.

For most probes several different kinetic parametrizations gave approximately optimal fits to the experimental data. Therefore it was important to consider if suboptimal parametrizations would also support the trends observed (Figure 7). To assess this, we plotted log P_{ap}(cyto) against log P_{ap}(ves) for slightly suboptimal curve fits. On the basis of the plots, parameter values for suboptimal solutions tend to cluster around the parameter values derived from the optimal solution. Within each probe, the inverse relationship between log P_{ap}(cyto) and log P_{ap}(ves) values is maintained, and the overall trend between log P_{ap}(cyto) and log P_{ap}(ves) continues to hold even for suboptimal parametrizations.

Discussion

The results presented here have important implications for cell-based drug transport and uptake assays. Without evidence for cytoplasmic small molecule sequestration, the concentration of drug molecules in the cytosol can be assumed to be equal to the concentration of drug in the entire cell. However, if small molecules become sequestered in subcellular compartments, this assumption becomes untenable. Prior to the present study, sequestration has generally been considered as a function of pH: for example, the trapping of ionized weak bases in acidic vesicles.[9,22−24] Yet, our results suggest that sequestration in intracellular vesicles is a phenomenon that can be easily influenced simply by adding or removing a methyl, ethyl, or isopropyl group from a molecule.

The present study is also important because it highlights the usefulness of employing combinatorial libraries of fluorescently tagged compounds to extract statistically meaningful information about subcellular transport properties. Because the fluorescent group is constant in all compounds analyzed, differences in subcellular localization represent differences in transport kinetics associated with chemical modifications of the triazine moiety. Moreover, statistically significant trends can be observed across the dataset, in a manner that would not be evident if a single compound had been used in the experiments. Last, fluorescence allows one to directly visualize transport dynamics in living cells, whereas other analytical methods can only be applied to reveal localization indirectly.

Interestingly, when log P_{ap}(cyto) was plotted against log P_{ap}(ves), a general trend became apparent across the entire dataset: to the extent that a molecule preferentially partitions from the cytosol to extracellular medium, it also preferentially partitions from the cytosol to intracellular vesicles. Had we not tested a combinatorial library of fluorescent compounds, this general organizing principle underlying subcellular transport dynamics would not be evident. The sequestration of small molecules in intracellular vesicles may be influenced by recycling of plasma membrane transporters in endocytic vesicles, or may reflect the activity of newly synthesized transporter molecules in exocytic vesicles on their way to the plasma membrane.[9−12] Alternatively, saturable or nonsaturable binding of probe to vesicle components[5,6,13] could also play a role in determining sequestration.

Is sequestration a phenotypic characteristic of the particular experimental system we have studied, or is it a universal transport phenomenon? The approach presented here is a first step toward studying the effects of chemical structure on

(22) Simon, S.; Roy, D.; Schindler, M. Intracellular pH and the control of multidrug resistance. *Proc. Natl. Acad. Sci. U.S.A.* **1994**, *91*, 1128−1132.

(23) Raghunand, N.; Martinez-Zaguilan, R.; Wright, S. H.; Gillies, R. J. pH and drug resistance. II. Turnover of acidic vesicles and resistance to weakly basic chemotherapeutic drugs. *Biochem. Pharmacol.* **1999**, *57*, 1047−1058.

(24) Martinez-Zaguilan, R.; Raghunand, N.; Lynch, R. M.; Bellamy, W.; Martinez, G. M.; Rojas, B.; Smith, D.; Dalton, W. S.; Gillies, R. J. pH and drug resistance. I. Functional expression of plasmalemmal V-type H+-ATPase in drug-resistant human breast carcinoma cell lines. *Biochem. Pharmacol.* **1999**, *57*, 1037−1046.

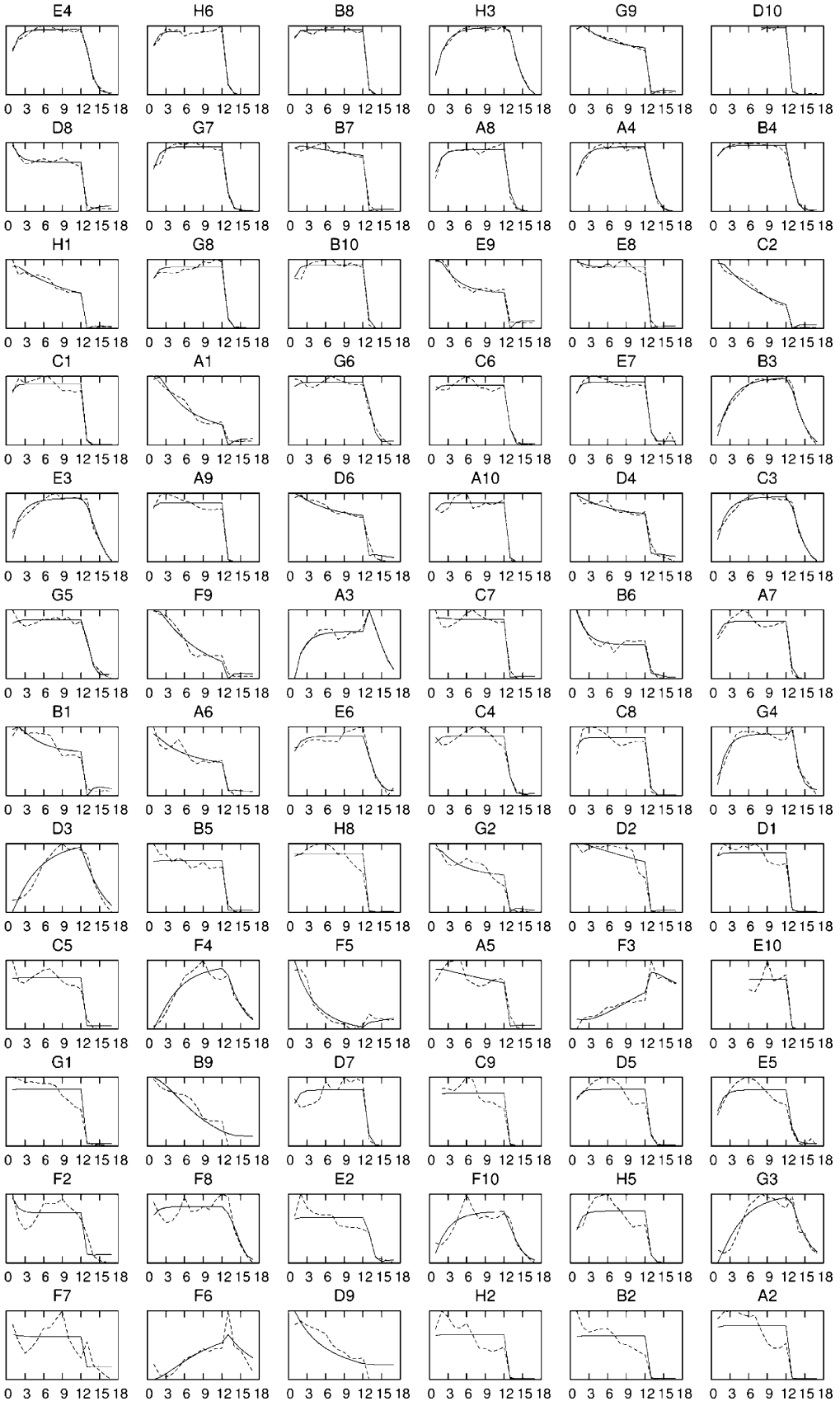

Figure 5. Kinetic traces of measured CV values (dashed curves, observed values; solid curves, fitted values). All traces have been normalized relative to the highest CV values in each kinetic trace, for clarity. Time points 1−12 were acquired in the presence of extracellular probe, and 13 onward were acquired in the absence of extracellular probe.

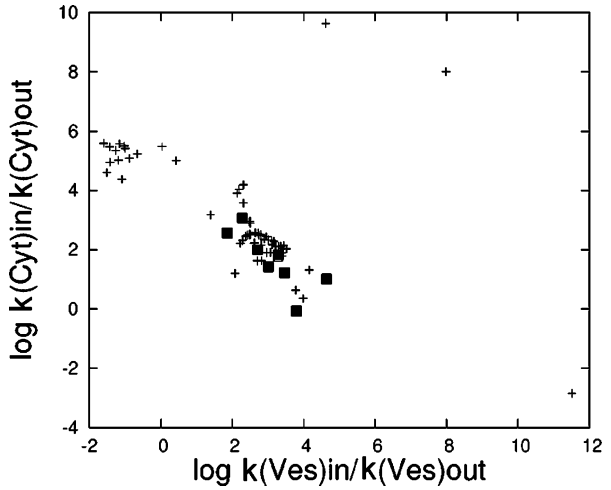

Figure 6. Calculated P_{ap}(cyto) and P_{ap}(ves) values are related. Plotting the log ratio of the partition coefficients of the probes examined reveals a strong, negative correlation between log P_{ap}(cyto) and log P_{ap}(ves). Filled boxes indicate molecules derivatized with the $R_1 = 3$ group, showing some of the highest P_{ap}(ves) values for all the probes, consistent with probe retention observed under efflux conditions (Figure 3).

subcellular sequestration and transport. Nevertheless, it establishes the usefulness of kinetic, high content screening instrumentation as an experimental system that may ultimately increase our ability to model and predict the absorption, distribution, metabolism, and excretion of small molecule drugs[25] in the living organism. In cancer cells, our observations could have important implications for understanding the accumulation of small molecules in tumor cells, targeted cytotoxicity and drug resistance,[26,27] and its potential relationship with membrane trafficking pathways involved in plasma membrane recycling and turnover.[28]

Irrespective of the actual transport mechanisms driving probe sequestration into intracellular vesicles, our observations challenge the extent to which the permeability of cells can be simply equated with the permeability of the plasma membrane. The partitioning of probes from the extracellular medium to the cytosol, and from cytosol to intracellular vesicles, indicates that viewing cells as single-compartment systems can obscure a role of intracellular membrane dynamics in cell permeability properties. Indeed, the cytoplasm is generally rich in endocytic or exocytic vesicles involved in plasma membrane recycling. Previous reports of active transporter molecules present in association with the membrane of cytoplasmic vesicles suggest that transport properties of intracellular vesicles and plasma membrane may be related.[14] Recycling and fusion of intracellular vesicles with the plasma membrane could lead to exocytic recycling of sequestered molecules back to the extracellular medium, which could limit transcellular transport irrespective of the plasma membrane's permeability properties.

Arguably, the ability to parametrize the behavior of fluorescent probes in terms of kinetic and imaging variables should enable more detailed analysis of small molecule transport pathways in living cells. Using combinatorial libraries of fluorescently tagged molecules,[19,20,29] the results presented here build upon recent advances in instrumentation, experimental design, and quantitative analysis techniques[30,31] that should allow for analysis of the system dynamics of subcellular transport in vivo, in relation to chemical structure and physicochemical properties. While the value of the systems approach has been advocated for studying the spatiotemporal regulation of gene expression, embryonic development, signal transduction, cell cycle, and other dynamics,[32−34] we propose that such an approach should also be applied for studying the biological basis of intracellular transport phenomena. Building on our previous work establishing relationships between chemical structure of small molecules and subcellular distribution,[20,29,35] the ability to calculate kinetic variables determining transport properties from image data will ultimately allow detailed analysis of small molecule transport pathways, and their relationship to the expression and localization of transporter proteins at the plasma membrane and at the membrane of internal organelles.

(25) Rowland, M.; Towzer, T. N. *Clinical Pharmacokinetics Concepts and Applications*; Lippincott Williams & Wilkins: Philadelphia, PA, 1995.

(26) Davis, S.; Weiss, M. J.; Wong, J. R.; Lampidis, T. J.; Chen, L. B. Mitochondrial and plasma membrane potentials cause unusual accumulation and retention of rhodamine 123 by human breast adenocarcinoma-derived MCF-7 cells. *J. Biol. Chem.* **1985**, *260*, 13844−13850.

(27) Jain, R. K. Delivery of molecular medicine to solid tumors: lessons from in vivo imaging of gene expression and function. *J. Controlled Release* **2001**, *74*, 7−25.

(28) Larsen, A. K.; Escargueil, A. E.; Skladanowski, A. Resistance mechanisms associated with altered intracellular distribution of anticancer agents. *Pharmacol. Ther.* **2000**, *85*, 217−229.

(29) Shedden, K.; Brumer, J.; Chang, Y. T.; Rosania, G. R. Chemoinformatic analysis of a supertargeted combinatorial library of styryl molecules. *J. Chem. Inf. Comput. Sci.* **2003**, *43*, 2068−2080.

(30) Song, Y.; Thiagarajah, J.; Verkman, A. S. Sodium and chloride concentrations, pH, and depth of airway surface liquid in distal airways. *J. Gen. Physiol.* **2003**, *122*, 511−519.

(31) Jayaraman, S.; Song, Y.; Vetrivel, L.; Shankar, L.; Verkman, A. S. Noninvasive in vivo fluorescence measurement of airway-surface liquid depth, salt concentration, and pH. *J. Clin. Invest.* **2001**, *107*, 317−324.

(32) Vilar, J. M.; Guet, C. C.; Leibler, S. Modeling network dynamics: the lac operon, a case study. *J. Cell Biol.* **2003**, *161*, 471−476.

(33) Ronen, M.; Rosenberg, R.; Shraiman, B. I.; Alon, U. Assigning numbers to the arrows: parameterizing a gene regulation network by using accurate expression kinetics. *Proc. Natl. Acad. Sci. U.S.A.* **2002**, *99*, 10555−10560.

(34) Surrey, T.; Elowitz, M. B.; Wolf, P. E.; Yang, F.; Nedelec, F.; Shokat, K.; Leibler, S. Chromophore-assisted light inactivation and self-organization of microtubules and motors. *Proc. Natl. Acad. Sci. U.S.A.* **1998**, *95*, 4293−4298.

(35) Rosania, G. R. Supertargeted chemistry: identifying relationships between molecular structures and their sub-cellular distribution. *Curr. Top Med. Chem.* **2003**, *3*, 659−685.

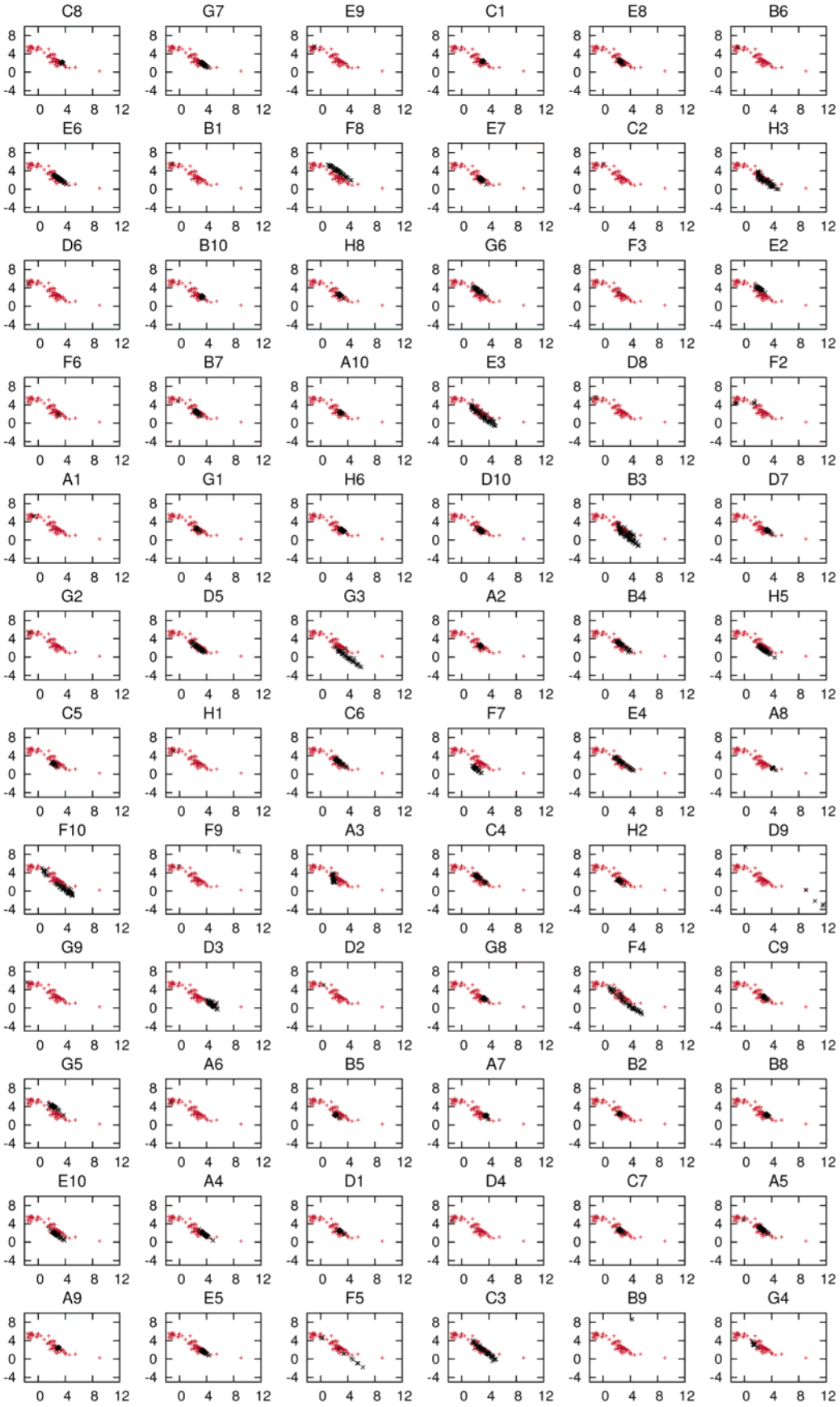

Figure 7. Plots of suboptimal log P_{ap}(cyto) and log P_{ap}(ves) values obtained for each individual probe in the library (black symbols), in relation to the optimal log P_{ap}(cyto) and log P_{ap}(ves) values observed across all the compounds in the library (red symbols).

In conclusion, the characterization of intracellular transport pathways may ultimately allow us to tailor the pharmacokinetic properties of drugs with a degree of precision not previously possible. Given that most drug targets are proteins, and that proteins have highly restricted patterns of subcellular distribution, subcellular transport studies may ultimately help improve efficacy and decrease toxicity by facilitating the development of chemotherapeutic agents with targeted sites of action. The use of fluorescent probes of subcellular transport, combined with high-throughput imaging instrumentation, should facilitate exploration of subcellular transport pathways as routes for targeted drug delivery within a cell.

Acknowledgment. We thank P. Matsudaira and J. Evans of the Whitehead—MIT Bioimaging Center for use of the kinetic, high content screening instrument and laboratory facilities and D. Fleisher and R. Chandrasekaran for critical reading of the manuscript. This work was supported in part by an Upjohn-Vahlteich award and funds from the University of Michigan College of Pharmacy awarded to G.R.R., and by funds from the University of Michigan Pharmacological Sciences Training Program awarded to V.C. This publication was also made possible by NIGMS Grant GM07767. Its contents are solely the responsibility of the authors and do not necessarily represent the official views of NIGMS.

Supporting Information Available: Student's *t*-test comparing the CV values of different R_1 groups (Table S1), synthesis scheme of NBD-tagged triazine library (Figure S2), and flow diagram of image analysis algorithm used to measure perinuclear NBD pixel intensity distributions (Figure S2). This material is available free of charge via the Internet at http://pubs.acs.org.

MP049916T